Supplementary Information (SI) for Journal of Materials Chemistry A.

Supplementary material

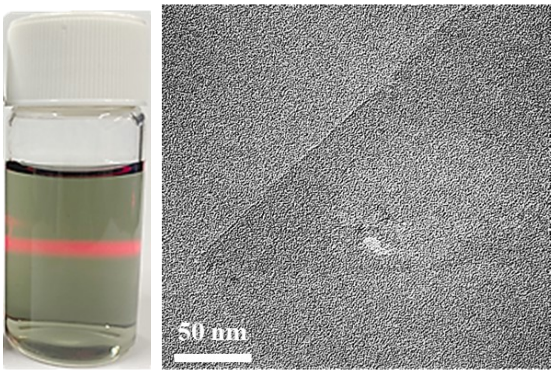

Fig. S1. Digital photograph and TEM image of MXene nanosheet. The TEM image shows the exfoliated single-layer MXene nanosheet with several hundred nanometers in lateral size.

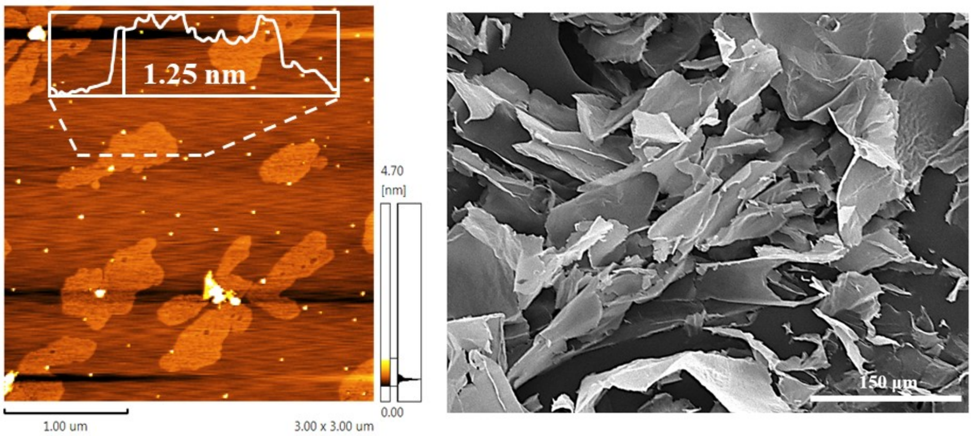

Fig. S2. AFM and SEM images of MXene nanosheet.

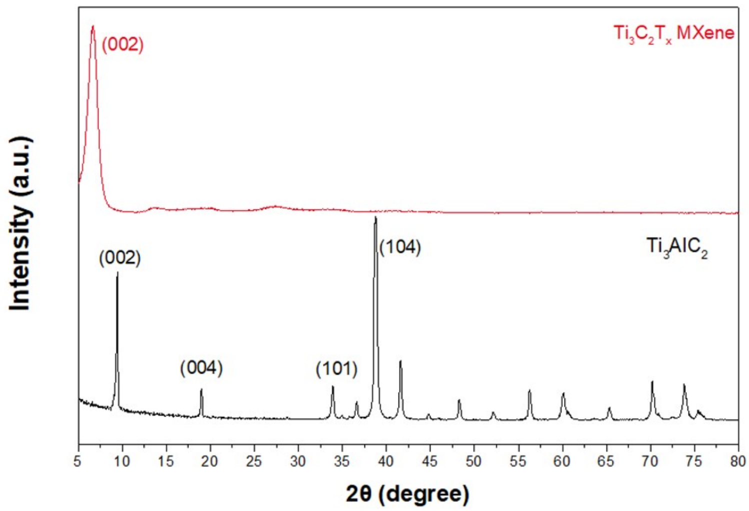

Fig. S3. XRD spectra of Ti_3AlC_2 and $Ti_3C_2T_x$ MXene.

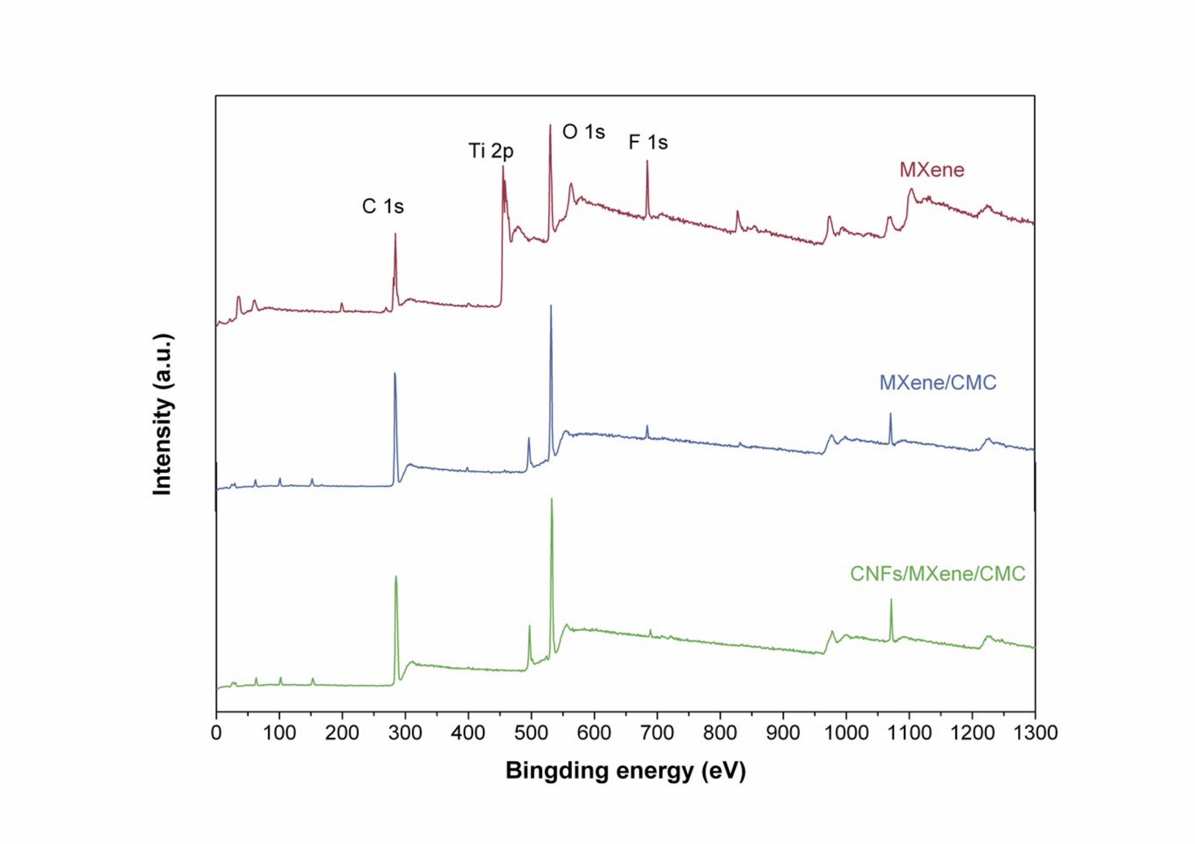

Fig. S4. XPS spectra of pure MXene, MXene/CMC, and CNFs/MXene/CMC.

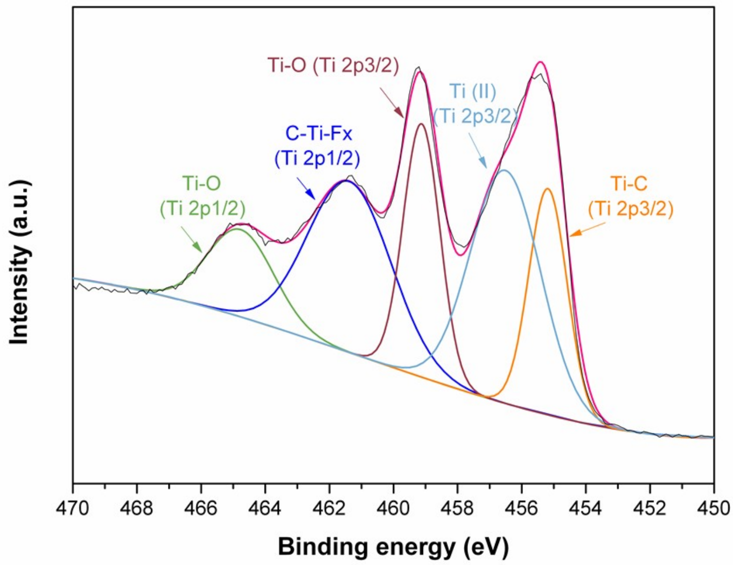

Fig. S5. Ti 2p XPS spectra of MXene.

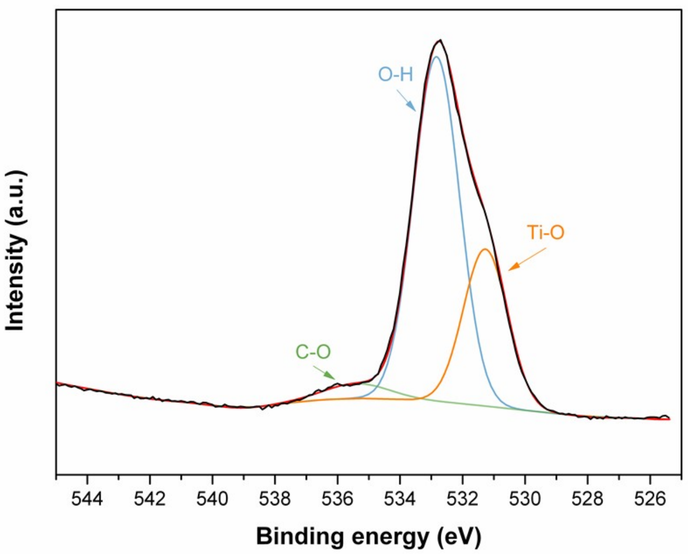

Fig. S6. O 1s XPS spectra of MXene

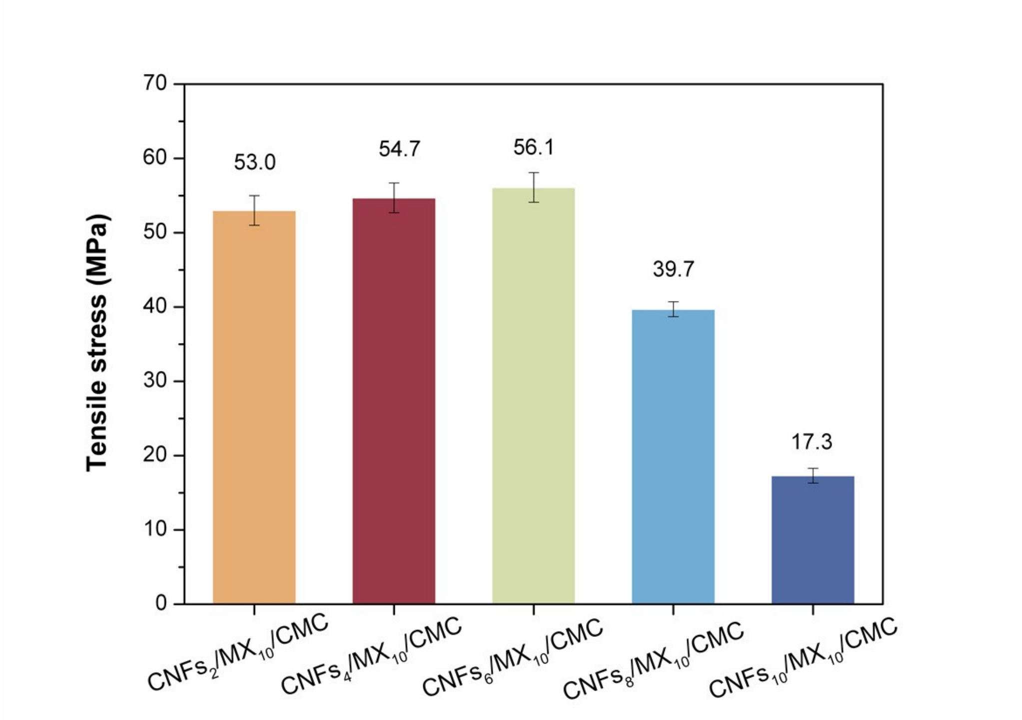

Fig. S7. Tensile stress of CNFs/MXene/CMC films containing 0, 2, 4, 6, 8 and 10 wt% CNFs.

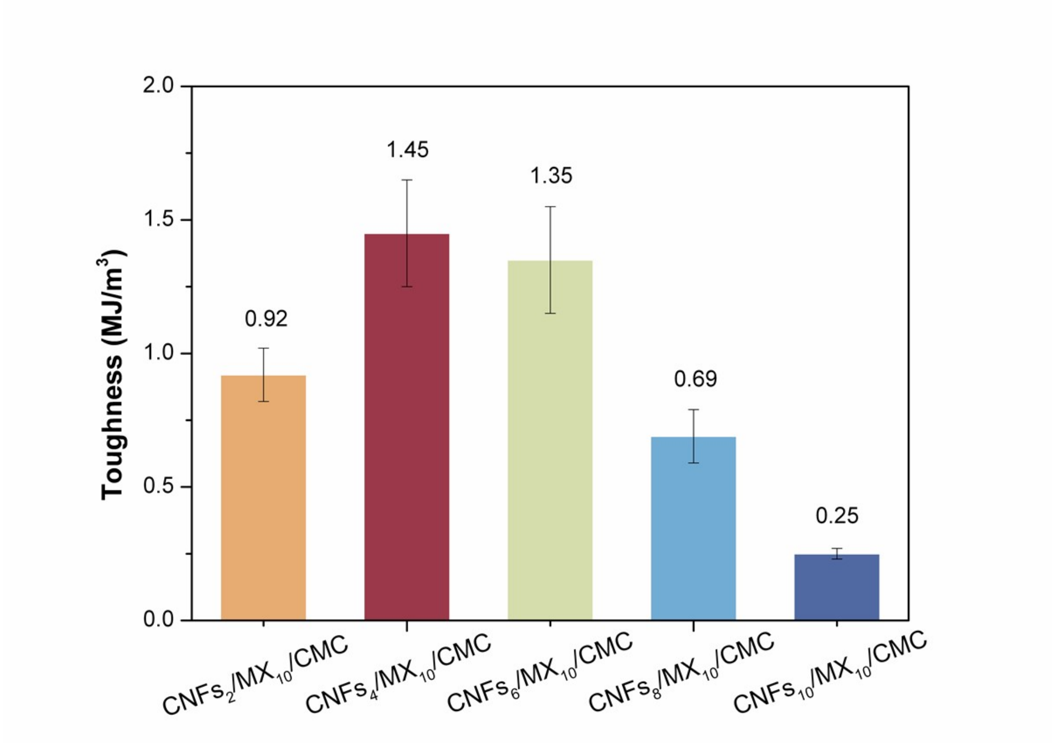

Fig. S8. Toughness of CNFs/MXene/CMC films containing 0, 2, 4, 6, 8 and 10 wt% CNFs.

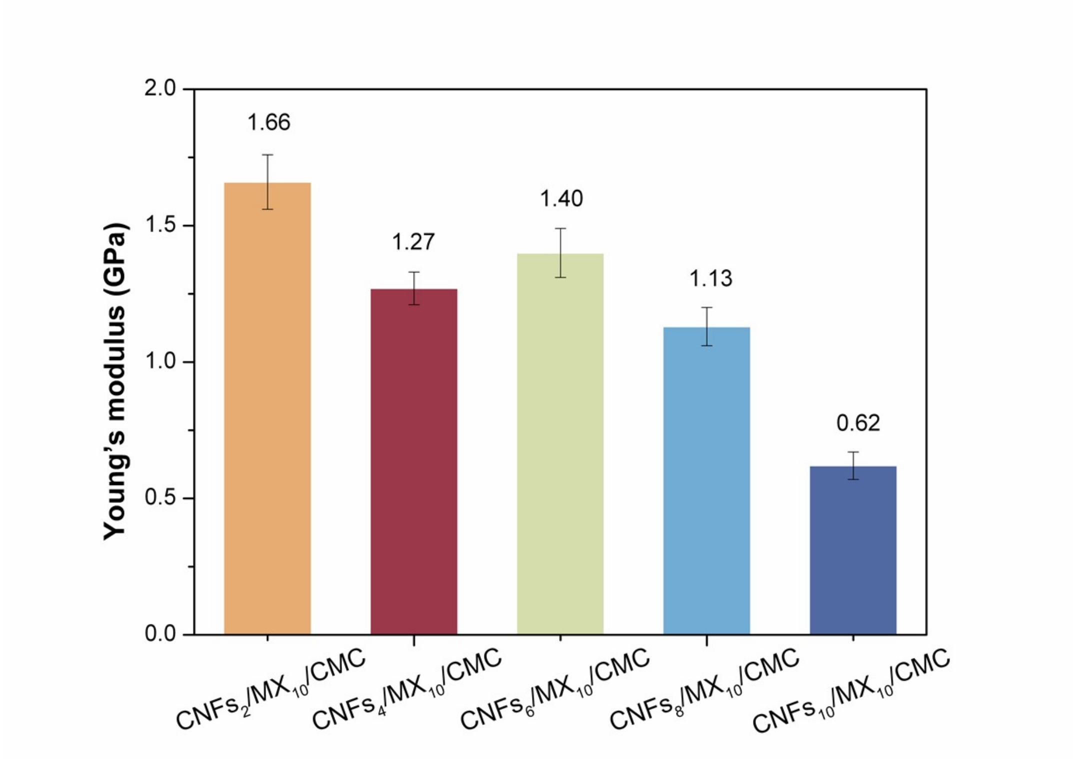

Fig. S9. Young's modulus of CNFs/MXene/CMC films containing 0, 2, 4, 6, 8 and 10 wt% CNFs.

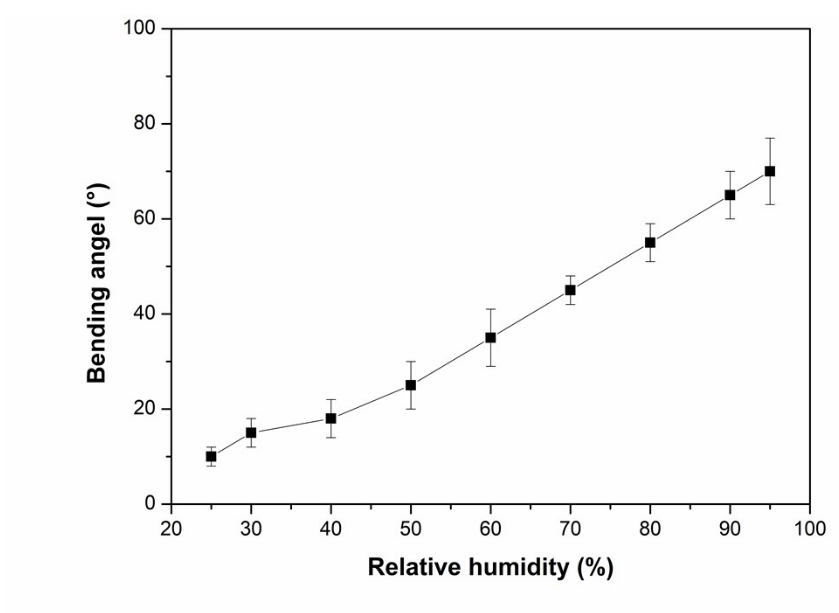

Fig. S10. The maximum bending angle of the pure MXene film at various relative humidity.

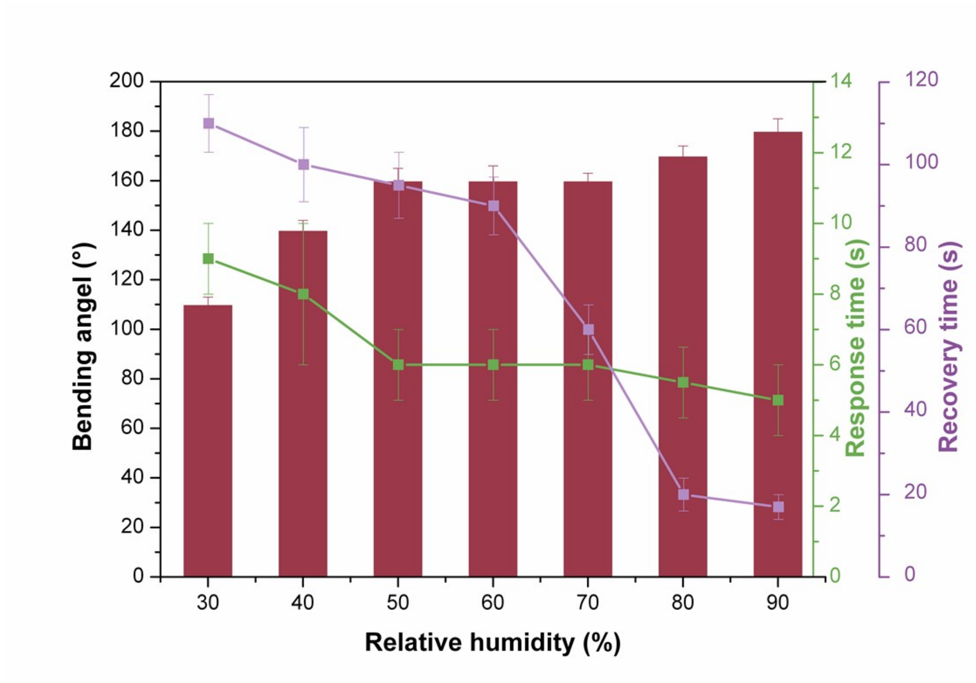

Fig. S11. Bending angles, response times and recovery times of MX_{10}/CMC film actuator at different relative humidity

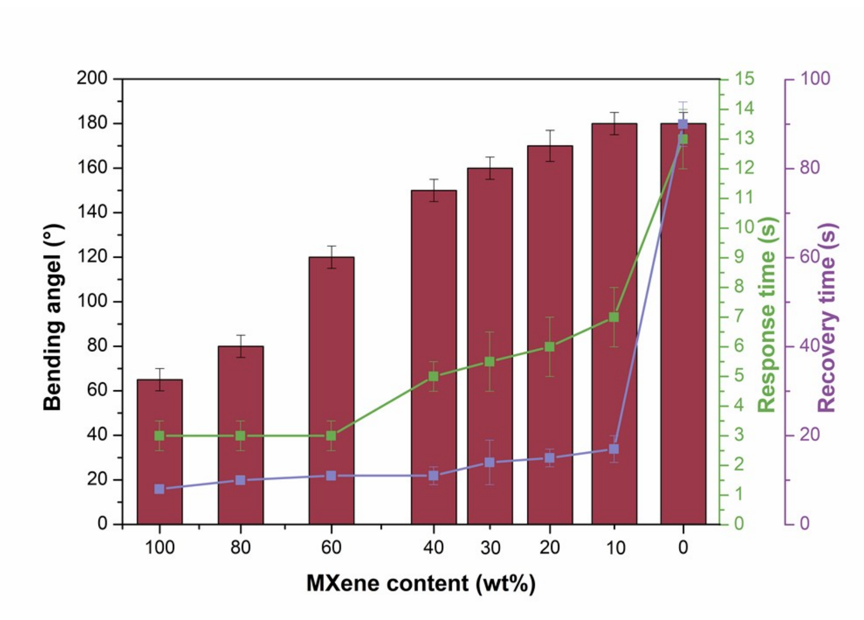

Fig. S12. Bending angles, response times and recovery times of MXene/CMC film actuators with different content of CMC at 95% relative humidity

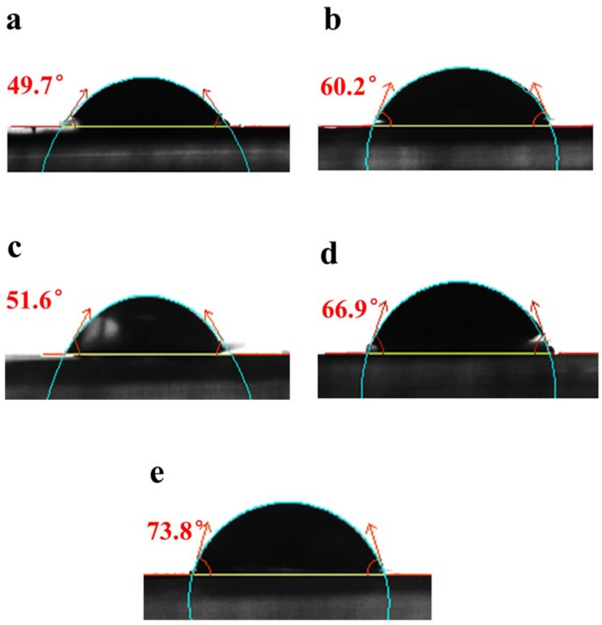

Fig. S13. Contact angle of different film (a) CMC, (b) MXene, (c) MX_{10}/CMC, (d) $CNFs_6$/MX_{10}/CMC-top, and (e) $CNFs_6$/MX_{10}/CMC-bottom

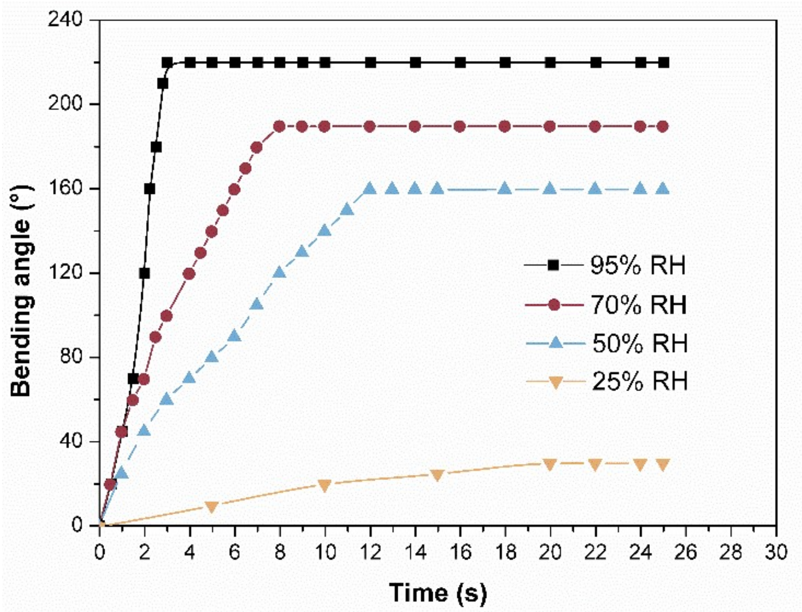

Fig. S14. The bending processes of the $CNFs_6/MX_{10}/CMC$ composite film under different relative humidity

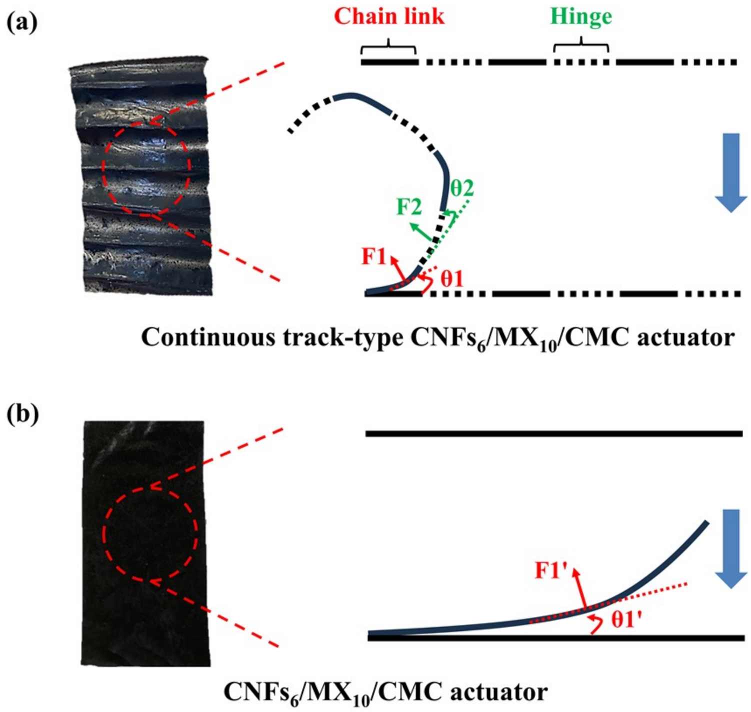

Fig. S15. Synchronous movement of bending angles of (a) continuous track-type and (b) flat $CNFs_6/MX_{10}/CMC$ actuator.

The relationship between deformation and force can be written as Equation (1):[1]

$$L\varepsilon = F/k_{eq} \tag{1}$$

where L is the length, ε is the strain, F is the Von mises stress applied to the structure, and k_{eq} is the equivalent stiffness coefficient.

Based on the finite element simulation results, it is evident that due to the similar material compositions of the flat and continuous track-type (chain link section) $CNFs_6/MX_{10}/CMC$ actuators, the Von Mises stresses generated by the humidity change are almost identical and are denoted as F1 and F1' respectively. Additionally, the force on the hinge section of the continuous track-type film, which is not uniformly distributed due to its anisotropic structure, is denoted as F2. The bending angles of the corresponding deformations resulting from the stresses are denoted as θ1, θ1', and θ2, respectively.

The bending angle of a continuous track-type $CNFs_6/MX_{10}/CMC$ actuator is determined by the deformation of neighboring sections. For one unit cell in periodic structures, the position of the end of the continuous track-type $CNFs_6/MX_{10}/CMC$ actuator in the coordinate system can be expressed as Equation (2):

$$\begin{cases} X = 0; \\ Y = L_1 \sin \theta_1 + L_2 \sin (\theta_1 + \theta_2) + \ldots + L_n \sin (\theta_1 + \theta_2 + \ldots + \theta_n); \\ Z = L_1 \cos \theta_1 + L_1 \cos (\theta_1 + \theta_2) + \ldots + L_n \cos (\theta_1 + \theta_2 + \ldots + \theta_n). \end{cases} \quad (2)$$

The position of the end of a flat $CNFs_6/MX_{10}/CMC$ actuator in the coordinate system can be expressed as Equation (3):

$$\begin{cases} X' = 0; \\ Y' = L \sin \theta_1'; \\ Z' = L \cos \theta_1', \end{cases} \quad (3)$$

where L is the length, θ is the bending angle.

Based on the results of finite element simulations and position calculations in the coordinate system, the continuous track-type actuator, owing to its distinctive structure of anisotropic film with periodic structures, exhibits a significantly larger bending angle compared to the flat one.

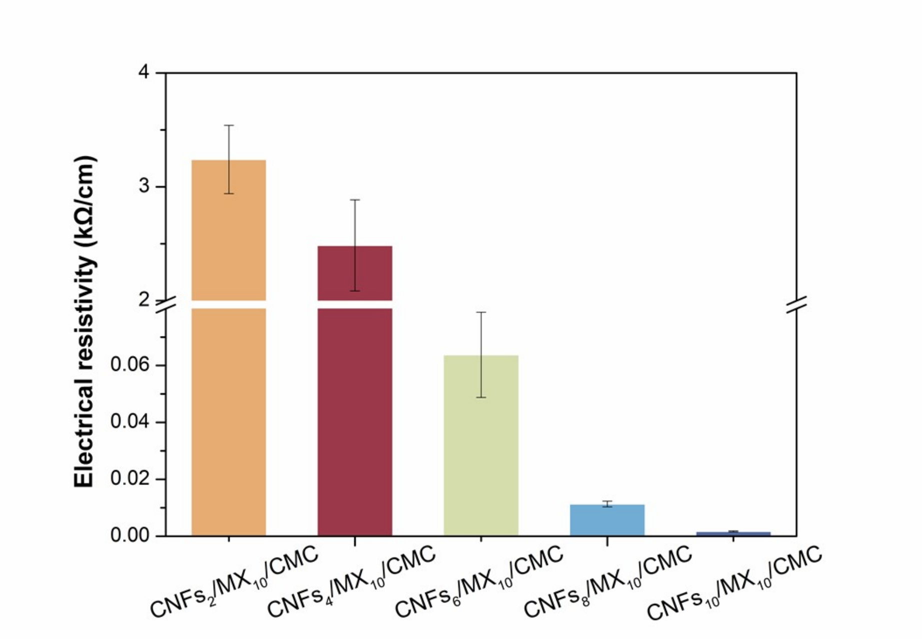

Fig. S16. Electrical resistivities of the CNFs/MX_{10}/CMC composite film with different content of CNFs.

Table S1. The mechanical properties of films

Sample	Tensile strength (MPa)	Strain breaking (%)	Toughness (MJ/m^3)	Young's modulus (GPa)
MXene	12.7±1.6	1.03± 0.05	0.050±0.003	1.3±0.2
CMC	93.3±2.1	7.34±0.06	4.49±0.68	1.28±0.1
MX_{10}/CMC	128.6±10.1	5.61±0.08	4.20±0.63	2.30±0.4
MX_{20}/CMC	105.7±5.8	4.57±0.04	2.49±0.32	2.23±0.3
MX_{40}/CMC	68.4±3.6	2.90±0.06	1.01±0.02	2.10±0.3
MX_{60}/CMC	29.1±1.9	2.42±0.03	0.23±0.01	1.21±0.1
$CNFs_2$/MX_{10}/CMC	53.0±2.3	3.22±0.07	0.92±0.12	1.66±0.1
$CNFs_4$/MX_{10}/CMC	54.7±2.1	4.31±0.08	1.45±0.19	1.27±0.06
$CNFs_6$/MX_{10}/CMC	56.1±1.9	4.14±0.08	1.35±0.18	1.4±0.09
$CNFs_8$/MX_{10}/CMC	39.7±1.4	3.53±0.04	0.69±0.14	1.13±0.07
$CNFs_{10}$/MX_{10}/CMC	17.3±1.2	2.84±0.03	0.25±0.02	0.62±0.05

Table S2. Comparison of MXene-based humidity actuators

Materials	Relative humidity difference (%)	Bending angle (°)	Response time/Recovery time (s)	Reference
GO/MXene	40-70	-100-245	20/20	2
MXene/CNF/PDA/BOPP	40-90	0-180	28/28	3
PDMM/BCNF	△40	176	1.6/3.8	4
MXene-graphene oxide film	40-90	160	5/19	5
Polydopamine-treated reduced graphene oxide/MXene film	△45	148	1/3	6
MXene/cellulose/PSSA composite membrane	20-97	28-130	15/20	7
CMC/MXene/Al^{3+} composite film	△20-△80	180	2/2.3	8
BC/GO/MXene composite film	△50	116	4/4	9
Continuous track-type CNFs/MXene/CMC	20-95	0-360	1.2/4.9	This work

GO: graphene oxide; CNF: cellulose nanofibrils; PDA: p-Phenylenediamine; BOPP: bidirectional oriented polypropylene; PDMM/BCNF: Polydopamine modified MXene/bacterial cellulose nanofiber; PSSA: polystyrene sulfonic acid; BC: Bacterial cellulose

References

1 Y. Lv, Q. Li, J. Shi, Z. Qin, Q. Lei, B. Zhao, L. Zhu and K. Pan, *ACS Appl. Mater. Interfaces*, 2022, **14**, 12434-12441.

2 L. Li, S. Zhao, X. J. Luo, H. B. Zhang and Z. Z. Yu, *Carbon*, 2021, **175**, 594-602.

3 J. Cao, Z. Zhou, Q. Song, K. Chen, G. Su, T. Zhou, X. Zhang, *ACS nano*, 2020, **14**, 7055-7065.

4 L. Yang, J. Cui, L. Zhang, X. Xu, X. Chen and D. Sun, *Adv. Funct. Mater.*, 2021, **31**, 2101378.

5 G. Jia, A. Zheng, X. Wang, L. Zhang, L. Li, C. Li and L. Cao, *Sensor. Actuat. B: Chem.*, 2021, **346**, 130507.

6 L. Yang, L. Zhang, J. Cui and D. Sun, *J. Mater. Chem. A*, 2022, **10,** 15785-15793.

7 P. Li, N. Su, Z. Wang and J. Qiu, *ACS nano*, 2021, **15**, 16811-16818.

8 J. Wei, S. Jia, C. Ma, J. Guan, C. Yan, L. Zhao and Z. Shao, *Chem. Eng. J.,* 2023, **451**, 138565.

9 Y. Ge, J. Zeng, B. Hu, D. Y. Yang, Y. and Shao, H. Lu, *Giant*, 2022, **11**, 100107.